



## Adsorption of methylene blue dye by pyrolytic tire char in fixed-bed column

V. Makrigianni<sup>a</sup>, A. Giannakas<sup>b</sup>, D. Hela<sup>c</sup>, M. Papadaki<sup>a</sup>, I. Konstantinou<sup>c,\*</sup>

<sup>a</sup>Department of Environmental and Natural Resources Management University of Patras, G. Seferi 2, Agrinio 30100, Greece, emails: makrigianni.v@gmail.com (V. Makrigianni), marpapadaki@upatras.gr (M. Papadaki)

<sup>b</sup>Department of Business Administration of Food and Agricultural Enterprises, University of Patras, Agrinio 30100, Greece, email: agiannakas@upatras.gr

<sup>c</sup>Department of Chemistry, University of Ioannina, Ioannina 45110, Greece, Tel. +30 2651008349; emails: iokonst@cc.uoi.gr (I. Konstantinou), dchela@cc.uoi.gr (D. Hela)

Received 22 June 2016; Accepted 29 October 2016

---

### ABSTRACT

The adsorption of methylene blue (MB) dye from aqueous solutions using acid-treated pyrolytic tire char in a fixed-bed adsorption column has been studied. The adsorbent was characterized by X-ray diffraction, specific surface area, Fourier transform infrared spectroscopy, elemental analysis, Boehm titration,  $\text{pH}_{\text{pzc}}$  and scanning electron microscopy. The effects of dye concentration and feed flow rate have been studied. Breakthrough curves and characteristic parameters of the column have been determined and modeled according to Adams–Bohart, Yoon–Nelson and Thomas models. Error analysis (average relative error) and  $R^2$  values for each model showed that MB adsorption was fitted better to Yoon–Nelson model followed by Thomas model. Desorption of MB for the reuse of the column can be performed with 0.1 M  $\text{HNO}_3$  solution while more than 64% of the initial adsorption capacity can be retained after three adsorption cycles. Considering the ample waste tire feedstock and the waste tire pyrolysis management needs, tire char can be a promising low-cost adsorbent for MB removal.

*Keywords:* Waste tires; Pyrolytic char; Adsorption; Desorption; Fixed-bed column; Models

---

### 1. Introduction

Environmental pollution from waste effluents has been seriously increased with the rapid development of industries [1]. Among various industrial wastewaters, dyes derived from textile finishing, dying, paper, hair coloring, cotton and rubber can cause harmful effects on the aquatic life as well as on human beings [2]. Methylene blue (MB) is the most commonly used cationic dye, with wide applications including coloring paper, cottons and wool dyeing, and stocks marking, and as a result, it constitutes also an environmental pollutant [3,4].

Industrial effluents containing MB require appropriate treatment before discharge. Due to the complex aromatic structure of dyes, their treatment in such wastewaters is very difficult. A range of conventional methods have been

employed for the treatment of MB-containing wastes, which include adsorption [5], biological treatments [6] and oxidation [7]. Adsorption has been found to be a highly efficient technique for the removal of organic/inorganic and toxic pollutants due to its simplicity of operation and its low cost [5,8]. Adsorption capacities from batch studies are useful in providing information about the effectiveness of dye-adsorbent system and the form of isotherms [9]. However, the data under batch conditions are usually obtained in the laboratory for the treatment of small volume of effluents, and they are not useful in general for direct application on industrial-scale treatment. On the other hand, experimental data obtained from laboratory or semi-pilot-scale fixed-bed columns can provide valuable information for the design and operation of pilot and industrial-scale water treatment processes. As such, they are of great value for applications dealing with the removal of dyes from aqueous solutions

---

\* Corresponding author.

[1,10]. In order to optimize the column operation, the modeling and simulation of the dynamic behavior of a fixed-bed column have been considered necessary. Successful design of a column adsorption process requires prediction of the shape of breakthrough curve for the effluent based on several models such as Adams–Bohart, Yoon–Nelson and Thomas [11]. From the industrial point of view, the removal of dyes and/or colored compounds in fixed-bed columns is an efficient process because of the adaptability of column systems to versatile processes and their easy handling [8].

The use of activated carbons and chars produced by pyrolysis of tire rubber for the removal of dyes, heavy metal ions and other organic pollutants from aqueous solutions by batch adsorption experiments has been reported previously in many studies [12–16]. Pyrolysis process involves thermal decomposition of waste tires at high temperatures (450°C–900°C) under oxygen-free atmosphere. Pyrolysing the tire waste materials could be a viable management alternative because it leads to the production of oil and gas fractions and a solid residue, the pyrolytic tire char (PTC) [17,18]. Activated carbons are widely used as effective adsorbents for the treatment of dye wastewaters because of its high surface area and broad availability and variety; however, the relatively high cost of activated carbons limits their applicability in certain wastewater treatment applications [12,19]. Production of low-cost adsorbents derived from a broad range of waste such as an industrial waste, natural materials or agricultural by-products has become a goal of many researchers [20,21]. Such low-cost adsorbents have given satisfactory performance at laboratory-scale column for treatment of colored effluents [20,22–25].

Tire char, a rich carbon source, has been widely used as a potential precursor for the production of added-value porous adsorbent materials for wastewater treatments [26]. In our previous works, PTC after an extensive purification treatment with refluxed nitric acid followed by a calcination step was found to be an efficient adsorbent for the removal of organic compounds, such as MB dye [27], and phenol [27,28] from aqueous solutions. Additionally, tire pyrolytic chars and activated carbons have been previously studied in batch adsorption process for the removal of other organic contaminants as well as for the removal of heavy metals [29–32]. The results confirmed that the pyrolytic char offers substantial adsorption capacity for the removal of organic pollutants compared with other low-cost adsorbents.

Following the above, the novel elements of this work, which are not reported previously in the literature, are: (a) the textural and physicochemical characterization of the PTC sorbent material after only a mild acid treatment step; (b) the evaluation of the adsorption potential for the removal of MB dye from aqueous solutions using a fixed-bed continuous column; and (c) the study on the effects of operational parameters such as initial dye concentration and flow rate on the column adsorption performance as well as the kinetic modeling of the respective breakthrough curves, which can provide valuable information for the application in wastewater treatment units. The contained data would contribute significantly to the potential uses of tire pyrolytic chars that are the key factors for the economic sustainability of industrial tire pyrolysis units.

## 2. Experimental setup

### 2.1. Preparation of tire rubber pyrolytic char

The tire char was derived from the pyrolysis of used rubber tires at 450°C in oxygen-free atmosphere under vacuum for 4 h. In order to remove pyrolysis impurities from as-received PTC such as ZnS and PbS [17], 600 g of char were suspended in 1.5 L of 2 M HNO<sub>3</sub> solution and kept under stirring for 24 h. The char suspension was then filtered and washed several times with distilled water until neutral pH. The char that has been subjected to the above-mentioned process will be hereafter called CHTR (char treated).

### 2.2. Characterization of pyrolytic char (CHTR)

The physicochemical characterization of CHTR material included X-ray diffraction (XRD), Fourier transform infrared (FTIR) spectroscopy, determination of specific surface area (SSA) and pH<sub>pzc</sub> Boehm titration and elemental analysis. XRD pattern was obtained on a powder X-ray diffractometer (Brüker Advance D8) employing Cu K $\alpha$  radiation ( $\lambda = 1.5418$  Å) in the 2 $\theta$  range from 10° to 90° with a 2 $\theta$  resolution of 0.02°. Infrared spectra were recorded on GX Perkin-Elmer FTIR System. N<sub>2</sub> adsorption–desorption isotherms were obtained at 77 K using an Autosorb-1 (Quantachrome Instruments, FL, USA) porosimeter, and the SSA (S<sub>BET</sub>) was calculated using the Brünauer–Emmett–Teller (BET) method based on the adsorption data. Scanning electron microscopy (SEM) images were obtained using a JEOL JSM-6300 instrument. In addition, oxygen-containing surface functional groups that can affect the hydrophobic/hydrophilic and acidic/basic character of adsorbent have been determined by Boehm titration [33]. Elemental analysis (C, H, N and S) was performed using an elemental analyzer (PerkinElmer 2400 Series II) at 1.100°C. Oxygen content was determined by mass difference. The point of zero charge (pH<sub>pzc</sub>) of the adsorbent was determined using the mass titration technique [34].

### 2.3. Batch adsorption kinetics and column adsorption studies

Batch adsorption kinetic experiments were carried out in 200 mL Erlenmeyer flasks by mixing 10 mg of CHTR adsorbent with 100 mL of MB solutions with an initial concentration of 20 mg L<sup>-1</sup>. The solutions were kept under dark and stirring (600 rpm) at 26°C  $\pm$  1°C until reaching the adsorption equilibrium. At regular time intervals, aliquots were taken ( $\approx$ 2 mL) and filtered through a 0.45- $\mu$ m filter (HVLP, Millipore) in order to remove the adsorbent particles followed by spectrometric analysis. The equilibrium time was found to be established after 30–45 min. The pH of the solutions was 7.0  $\pm$  0.2. Four kinetic models including the pseudo-first-order, the pseudo-second-order, intraparticle diffusion and Elovich models [22] have been applied to fit the experimental data.

The dynamic adsorption studies were carried out in a cylindrical fixed-bed glass column with an inside diameter of 7.4 cm and 35 cm of height. An amount of about 300 g of CHTR was packed into the column on a glass wool support. Uniform inlet flow of the solution into the column was maintained by an inlet valve. MB solution with the selected initial concentration flowed from the top of the column via a vacuum pump at the desired flow rate, which was measured

with a flow meter. The MB stock solution holder was constantly agitated with a magnetic stirrer. Before the adsorption experiments, the bed was flushed several times with deionized water in order to avoid the formation of channels or cracks in CHTR particles by the influent flow through the column. Initial concentrations of 10, 20 and 40 mg L<sup>-1</sup> were tested at different flow rates of 50, 100 and 150 mL min<sup>-1</sup>. The bed length was 15 cm. The MB solutions at the outlet of the column were collected at regular time intervals, and the concentration ( $C_t$ ) was measured using a UV–Vis spectrophotometer (Hitachi, U-2000) at a wavelength of 540 nm. All the experiments were carried out at room temperature (26°C ± 1°C) at solution inherent pH (7.0 ± 0.2). Triplicate experiments were performed and reproducibility of the results as expressed by percentage relative standard deviation (% RSD) varied between 4% and 15%.

#### 2.4. Column desorption experiments

In order to recover the adsorbed MB dye and to reuse the exhausted columns, the regeneration of column after an adsorption cycle with 20 mg L<sup>-1</sup> MB initial concentration was carried out by 0.1 M HNO<sub>3</sub> or deionized water at flow rate of 100 mL min<sup>-1</sup>. Column effluent samples were collected at regular time intervals, and the concentration of MB was measured as described previously. After the recovery of the dye, the column was washed with deionized water before performing another adsorption cycle under the same experimental conditions. Three cycles of adsorption were performed.

#### 2.5. Analysis and modeling of column adsorption data

MB adsorption on CHTR was studied in terms of breakthrough curves expressed by the ratio of the outlet MB concentration to inlet MB concentration as a function of time ( $C_t/C_0$  vs. time,  $t$ ). The total adsorbed MB quantity,  $q_{\text{total}}$  (mg), in the column for a given inlet concentration and flow rate was calculated by Eq. (1):

$$q_{\text{total}} = \frac{Q}{1000} \int_{t=0}^{t=t_{\text{total}}} C_{ad} dt \quad (1)$$

where  $C_{ad}$  (mg L<sup>-1</sup>) is the adsorbed MB concentration (inlet dye concentration,  $C_0$  – outlet dye concentration,  $C_t$ );  $Q$  is the volumetric flow rate (mL min<sup>-1</sup>); and  $t_{\text{total}}$  is the total flow time (min).

Maximum capacity of the column or equilibrium dye uptake in the column ( $q_{\text{eq}}$ ) was defined by Eq. (2), as the quantity adsorbed ( $q_{\text{total}}$ ) per mass (g) of the adsorbent ( $m$ ) in the column:

$$q_{\text{eq}} = \frac{q_{\text{total}}}{m} \quad (2)$$

Adams–Bohart, Yoon–Nelson and Thomas models have been employed to describe the column adsorption behavior simulating the breakthrough curves for the effluent. The Adams–Bohart model [35] was applied for the description between  $C_t/C_0$  and  $t$  in a continuous system, especially the initial part of the breakthrough curve. This model is based on the surface reaction theory, and it assumes that equilibrium does

not take place instantaneously while the rate of the adsorption is proportional to the adsorption capacity of adsorbent and the concentration of the adsorbed substance. The equation of Adams–Bohart model is expressed as follows:

$$\frac{C_t}{C_0} = \exp\left(K_{AB}C_0t - \frac{K_{AB}N_0Z}{U_0}\right) \quad (3)$$

and the simplified linear form is:

$$\ln\frac{C_t}{C_0} = K_{AB}C_0t - K_{AB}N_0\frac{Z}{U_0} \quad (4)$$

where  $K_{AB}$  is the kinetic (mass transfer) constant (L mg<sup>-1</sup> min<sup>-1</sup>);  $U_0$  (cm min<sup>-1</sup>) is the linear velocity calculated by dividing the volumetric flow rate (mL min<sup>-1</sup>) by the column cross-sectional area (cm<sup>2</sup>);  $Z$  (cm) is the bed depth of column and  $N_0$  (mg L<sup>-1</sup>) is the saturation concentration or adsorption capacity.

Yoon–Nelson model [36] is considered as the less complicated column model because the characteristics of adsorbate, adsorbent and the physical properties of adsorption bed are not needed to be known in detail. It assumes that the rate of decrease in the probability of adsorbate sorption is proportional to the probability of adsorbate sorption and the probability of adsorbate breakthrough on the adsorbent.

The non-linear and linear forms of the Yoon–Nelson model for a single component system are expressed in the following Eqs. (5) and (6), respectively:

$$\frac{C_0}{C_t} = 1 + \exp(\tau k_{YN} - k_{YN}t) \quad (5)$$

$$\ln\left(\frac{C_0}{C_0 - C_t}\right) = k_{YN}t - \tau k_{YN} \quad (6)$$

where  $k_{YN}$  is the Yoon–Nelson velocity rate constant (min<sup>-1</sup>);  $\tau$  is the time required for 50% of adsorbate breakthrough (min) and  $t$  is the flow time (min).

The Thomas model is the most widely used one to describe the column adsorption performance [37]. The Thomas model assumes ideal plug flow with no axial dispersion in the bed and Langmuir adsorption–desorption equilibrium with the rate of driving force to obey second-order reversible reaction kinetics. Also, the intraparticle diffusion and external resistance during the mass transfer processes are considered to be negligible while sorption is not limited by the chemical reaction, but is controlled by the mass transfer at the interface. The model has the following form:

$$\frac{C_t}{C_0} = \frac{1}{1 + \exp\left(\frac{k_{Th}q_0m}{Q} - k_{Th}C_0t\right)} \quad (7)$$

and the linearized expression is given by Eq. (8):

$$\ln\left(\frac{C_0}{C_t} - 1\right) = \frac{k_{Th}q_0m}{Q} - k_{Th}C_0t \quad (8)$$

where  $k_{Th}$  is the Thomas rate constant (mL min<sup>-1</sup> mg<sup>-1</sup>);  $q_0$  is the predicted bed capacity at the equilibrium (mg g<sup>-1</sup>);

$m$  is the mass of adsorbent in the column (g);  $Q$  (mL min<sup>-1</sup>) is the feed flow rate and  $V$  is the effluent volume.

In order to evaluate the validity of the kinetic models' fitting to the experimental dynamic data, the average relative error (ARE) was determined according to the following equation:

$$\text{ARE} = \frac{\sum_{i=1}^n |(C_i/C_0)_{\text{exp}} - (C_i/C_0)_{\text{cal}}|}{n} \times 100\% \quad (9)$$

where  $n$  is the number of measurements, and  $(C_i/C_0)_{\text{exp}}$  and  $(C_i/C_0)_{\text{cal}}$  are the experimental and the predicted by the model normalized concentrations, respectively.

### 3. Results and discussion

#### 3.1. Characterization of the pyrolytic char adsorbent

Table 1 shows the physicochemical characteristics for CHTR, including XRD,  $\text{pH}_{\text{pzc}}$ , SSA, elemental analysis and surface oxygen functional groups by Boehm titration. Fig. 1 shows the XRD pattern of CHTR in the scan range of 10°–90°. An amorphous nature of the product both with the main reflection ((002), (100), (101) planes) of graphite carbon 2H (Space group P 63mc, hexagonal crystal system) was identified.

The adsorption–desorption isotherms of N<sub>2</sub> at 77 K for CHTR are presented in Fig. 2. The N<sub>2</sub> adsorption was very limited without a considerable hysteresis loop. The corresponding SSA was found to be  $S_{\text{BET}} = 15 \text{ m}^2 \text{ g}^{-1}$ . In such cases, no attempt to determine the pore size distribution is worth the effort, since the major porosity is external between solid particles, which do not possess considerable internal pore surface area. The surface area of CHTR is lower than those reported in literature, where many researchers produced materials by pyrolysis of raw tires with mesoporous structure and surface areas in the range 54–87 m<sup>2</sup> g<sup>-1</sup> [38,39]. Different pyrolysis conditions such as temperature and time have an effect on the porosity of the tire rubber carbon [5] or the presence of possible inorganic impurities, which may block the pores leading to a reduced available surface area [40,41]. Miguel et al. [42] referred to the high mesoporosity of tire-derived samples, which is desirable for adsorption of large molecular-size compounds from solution. Hadi et al. [43] also found a low external surface area 32 m<sup>2</sup> g<sup>-1</sup>, with 0.2 cm<sup>3</sup> g<sup>-1</sup> total pore volume. The porosity developed was also studied by SEM analysis (Fig. 3). As it is illustrated, microporosity and mesoporosity were not developed in CHTR while big cavities between “stone” like particles (1–10 μm) correspond to macroporous/nonporous morphology denoted also by BET plots.

Moreover, the chemical nature and the amount of surface groups of the PTC were also taken into account. Results in

Table 1 present the Boehm titration [33] and elemental analysis of the CHTR. As shown in Table 1, the total acidic and phenolic groups of CHTR are 1.25 and 0.3 mmol g<sup>-1</sup> correspondingly, much lower than the values reported in our previous work [27] where an extra purification treatment has been applied. The acidic treatment of PTC is known to lead to demineralization of the char (in principal removal of sulfur and zinc) and to its oxidation (increase of oxygen content) [19]. The results from elemental analysis (see Table 1) indicate

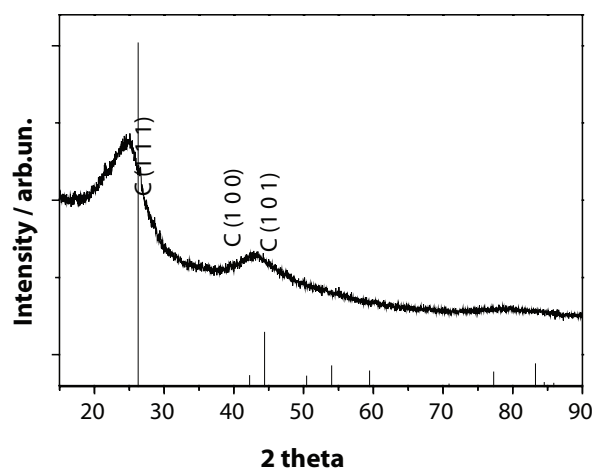


Fig. 1. X-ray diffraction (XRD) characterization for acid-treated pyrolytic char (CHTR).

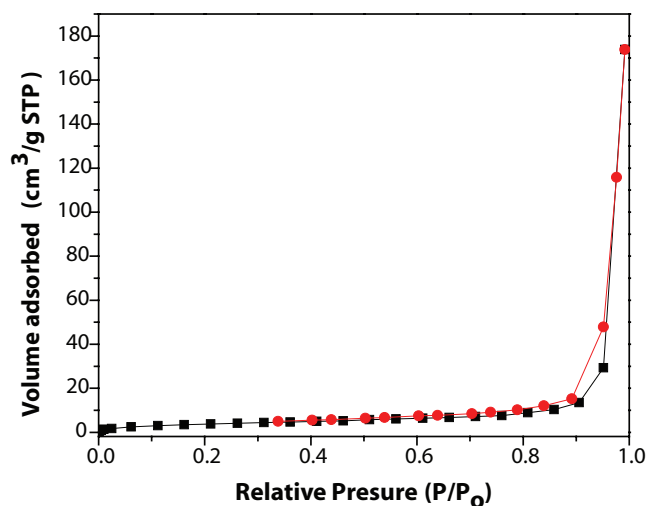


Fig. 2. N<sub>2</sub> adsorption–desorption isotherms on acid-treated pyrolytic char (CHTR).

Table 1

Results of XRD, point of zero charge, specific surface area, elemental analysis and surface chemistry of acid treated char

Adsorbent	XRD	$\text{pH}_{\text{pzc}}$	$S_{\text{BET}}$ (m <sup>2</sup> g <sup>-1</sup> )	Elemental composition (%) and atomic ratio							Surface functional groups (mmol g <sup>-1</sup> )				
				C	H	N	S	O	H/C	O/C	(O+N)/C	Carboxylic	Lactonic	Phenolic	Total acidic
CHTR	Amorphous/ Graphite	3.8	15	73.65	3.10	2.93	1.60	18.72	0.04	0.25	0.29	0.2	1.2	0.3	1.25

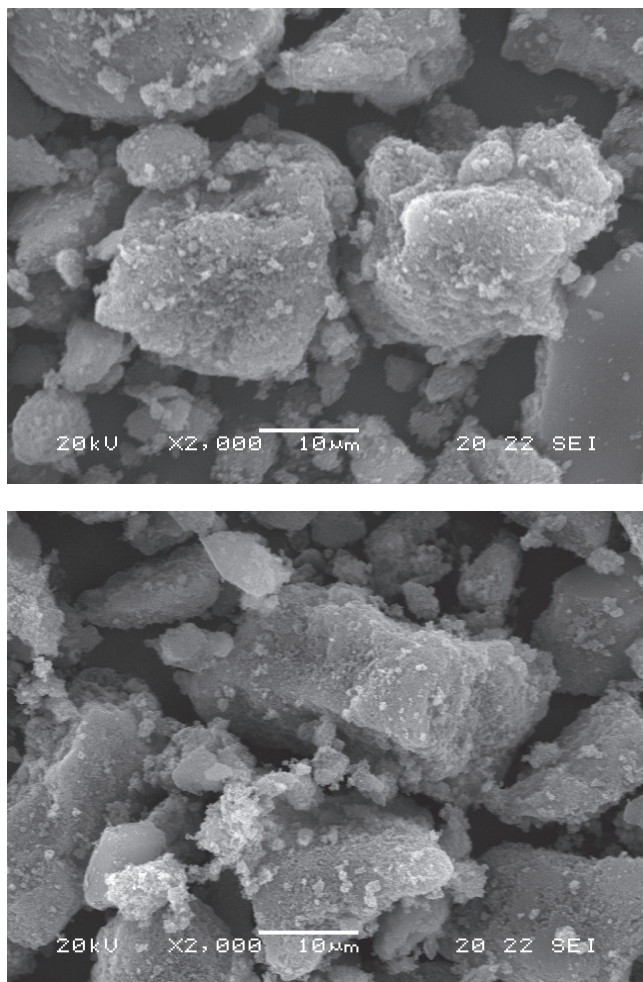


Fig. 3. SEM images of the acid-treated pyrolytic char (CHTR) adsorbent used in the column adsorption studies of MB.

high carbon and oxygen content, 73.65 and 18.72 wt%, respectively. Nitrogen, sulfur and hydrogen content were reduced as a result of the acidic process (2.93, 1.60 and 3.10 wt%, respectively). Several studies in the literature referred to chemical analysis of chars derived from tire pyrolysis. The chars presented high carbon contents of up to 90 wt%, high sulfur contents between 1.9 and 2.7 wt% and metals, mostly zinc. However, the acid treatment resulted in a char (CHTR) with higher oxygen content than chars reported in the literature [17,44–46]. As it is shown in Table 1, the aromatic index (H/C and O/C ratios) and the polarity index  $[(O + N)/C]$  [47] suggest that the surface of adsorbent becomes more hydrophilic upon treatment with nitric acid. CHTR had an acidic point of zero charge,  $\text{pH}_{\text{pzc}}$  of 3.8 after treatment with  $\text{HNO}_3$  as corroborated by the elemental analysis (Table 1). PTC with a  $\text{pH}_{\text{pzc}}$  lower than the pH of the solution (6.5–7.0) has a negative surface charge. Therefore, there is a strong attraction between negative adsorbent surfaces and cationic ions in solution [48].

In Fig. 4(a), the IR spectra of the CHTR material is shown. More specifically, the bands observed at 3,444, 1,704 and 1,095  $\text{cm}^{-1}$  for CHTR are assigned to  $\nu(\text{O-H})$  including hydrogen bonding,  $\nu(\text{C=O})$  and  $\nu(\text{C-O})$  stretching vibrations,

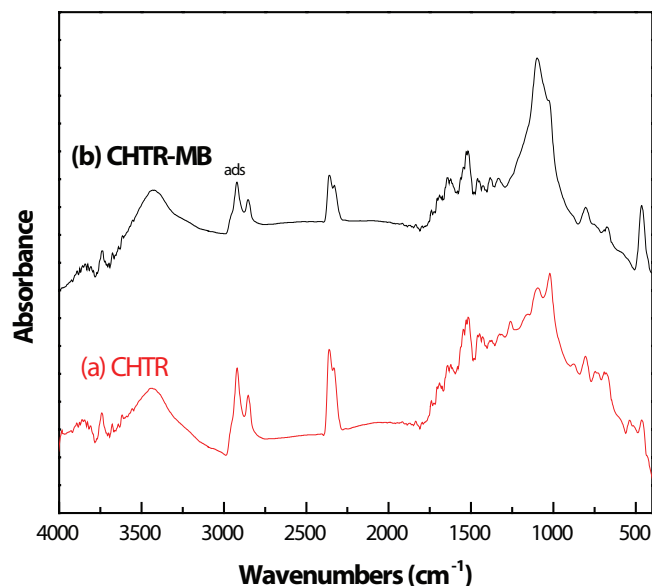


Fig. 4. FT-IR spectra of: (a) CHTR adsorbent and (b) CHTR adsorbent after MB adsorption ( $C_{\text{MB}} = 20 \text{ mg L}^{-1}$  and flow rate =  $10 \text{ mL min}^{-1}$ ).

respectively, while the band at 1,463  $\text{cm}^{-1}$  is attributed to C–O stretching vibration in carboxyl group [47,49], confirming the formation of carboxyl, lactonic and phenolic groups in the surface of the adsorbent, as also determined by Boehm titration. In the region of the  $\nu(\text{C-O})$  vibration, not only oxygen surface groups and structures of CHTR but also other inorganic components such as  $\text{SiO}_2$  presented at the starting pyrolytic char may cause absorption of infrared radiation [30]. The band at 2,358  $\text{cm}^{-1}$  is attributed to  $\text{C}\equiv\text{C}$  stretching vibration in alkyne group [47,50]. The peaks in the range of 1,600–1,480  $\text{cm}^{-1}$  were assigned to the  $\text{C}=\text{C}$  stretching vibrations of various aromatics and polynuclear aromatics structure on the surface of CHTR [51]. Finally, the bands at 2,919 and 2,852  $\text{cm}^{-1}$  corresponded to  $\nu(\text{C-H})$  stretching vibration.

In order to illustrate interaction between MB and CHTR, FTIR analysis of CHTR after MB adsorption was also investigated and shown in Fig. 4(b). According to previously reported FTIR spectrum of MB, stretching vibration of tertiary amine groups is observed at 3,422  $\text{cm}^{-1}$  while bands corresponding to the C–H stretching vibration are at 2,919 and 2,852  $\text{cm}^{-1}$  [52]. After the dye adsorption onto CHTR, the peaks at 3,444, 2,360, and 1,072  $\text{cm}^{-1}$  are shifted to 3,430, 2,358 and 1,066  $\text{cm}^{-1}$  while peak at 1,097  $\text{cm}^{-1}$  became more intense suggesting the interactions of dye molecules with the functional groups of pyrolytic sorbent.

The adsorption kinetics of MB dye onto CHTR is shown in Fig. 5. As it can be observed, the adsorption of MB is a fast process, and the equilibrium was found to be established after only 30–45 min. The experimental data fitted better to the pseudo-second-order model ( $R^2 = 0.9996$ ) with  $q_{e,\text{exp}} = 6.51 \text{ mg g}^{-1}$  and a rate constant  $k_2 = 0.12 \text{ g mg}^{-1} \text{ min}^{-1}$ .

### 3.2. Effect of inlet MB concentration on breakthrough curves

Adsorption experiments were carried out in the fixed-bed column previously described at varying dye-influent

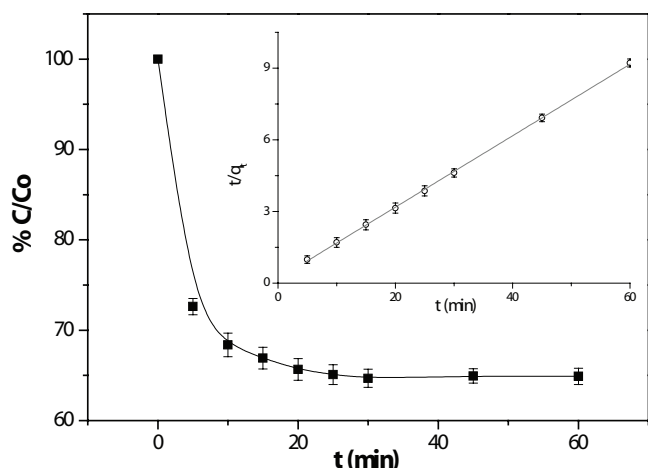


Fig. 5. Adsorption kinetics onto CHTR adsorption (inset: fitting of the experimental data to the linear form of pseudo-second-order kinetic model).

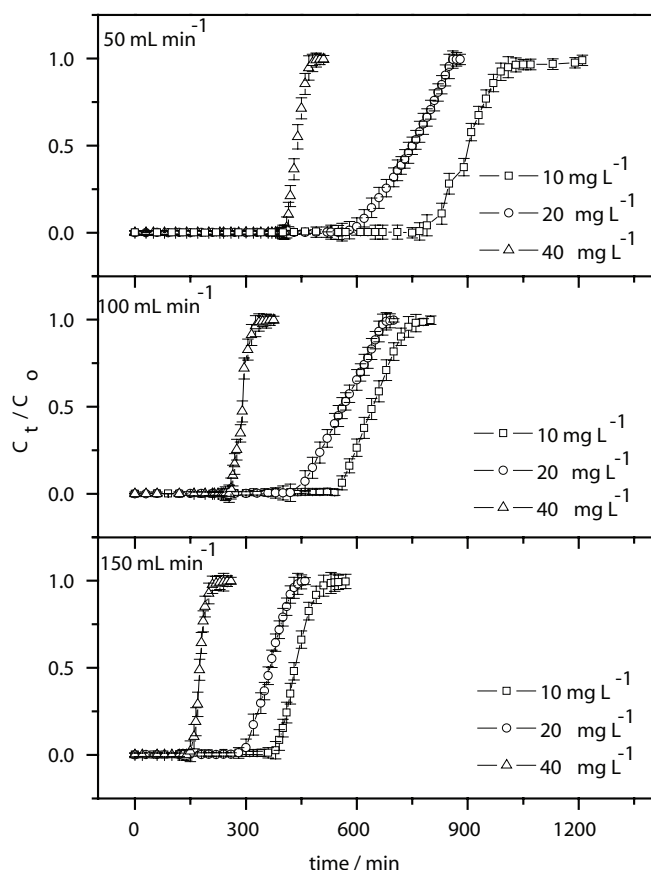


Fig. 6. Effects of various initial MB concentrations ( $\text{mg L}^{-1}$ ) on the breakthrough curves at different flow rates: (a)  $50 \text{ mL min}^{-1}$ , (b)  $100 \text{ mL min}^{-1}$  and (c)  $150 \text{ mL min}^{-1}$ .

concentrations ( $10, 20$  and  $40 \text{ mg L}^{-1}$ ) in a fixed adsorbent bed height of  $15 \text{ cm}$  and at flow rates of  $50, 100$  and  $150 \text{ mL min}^{-1}$ . Fig. 6 shows the breakthrough curves of MB sorption at different initial concentrations and flow rates. The total adsorbed MB quantities ( $q_{\text{total}}$ ), equilibrium MB

uptake ( $q_e$ ), breakpoint time ( $t_b$ ) and exhaustion time ( $t_e$ ) are presented in Table 2. The breakpoint time decreased with increasing inlet MB concentration as the adsorption sites were saturated rapidly by dye molecules in the system. As can be clearly seen in Fig. 6 and Table 2, an increase in the initial dye concentration from  $10$  to  $40 \text{ mg L}^{-1}$  resulted in a decrease of breakthrough time from  $760$  to  $150 \text{ min}$ . As the inlet dye concentration increased, sharper breakthrough curves were obtained, indicating that adsorption sites were occupied much faster and lower volume of solution could be treated [53]. The highest adsorption capacity was obtained for  $40 \text{ mg L}^{-1}$  MB initial concentration, with an adsorption capacity of  $3.85 \text{ mg g}^{-1}$ . The fact that higher adsorption capacities were achieved in the column with a higher MB concentration may be explained by the increase of occupied adsorption sites as the MB concentration increases as well as by the high concentration difference, which provides a high driving force for the adsorption process [54]. These results demonstrated that the change of concentration gradient affected the saturation rate and breakthrough time, or in other words, the diffusion process was concentration dependent [55]. Therefore, a decrease in initial concentration gave an extended breakthrough curve, indicating that a higher volume of dye solution could be treated. This was due to the fact that a lower concentration gradient caused a slower transport because of a decreased diffusion coefficient or decreased mass transfer coefficient [3,54].

### 3.3. Effect of flow rates on breakthrough curves

The breakthrough curves at various flow rates ( $50, 100$  and  $150 \text{ mL min}^{-1}$ ) for three different initial MB concentrations ( $10, 20$  and  $40 \text{ mg L}^{-1}$ ) are shown in Fig. 7. As can be seen, at higher flow rates, the breakthrough curves became steeper while the breakthrough point and exhausted time were observed sooner. The variation in the slope of the breakthrough curve and adsorption capacity is likely to occur because at higher flow rates the mass-transfer rate increases. This behavior indicates that the residence time of the MB solution in the column is insufficient and diffusion resistance of MB into the pores of CHTR does exist or more probably the number of adsorption sites is insufficient [56,57]. The column was found to perform better at a lower flow rate of influent that resulted in a longer breakthrough and exhausted time because MB had more time for diffusion and interaction between the dye molecules and char adsorption sites, which resulted in a higher removal of MB molecules. The total adsorbed MB quantity ( $q_{\text{total}}$ ), equilibrium MB uptake ( $q_e$ ), breakpoint time ( $t_b$ ) and exhaustion time ( $t_e$ ) at different flow rates are shown in Table 2. The maximum bed capacity ( $q_e$ ) was found  $3.85 \text{ mg g}^{-1}$  at initial MB concentration of  $40 \text{ mg L}^{-1}$  for the flow rate of  $100 \text{ mL min}^{-1}$ . As can be also observed in Table 2, when the flow rate increases from  $50$  to  $100 \text{ mL min}^{-1}$ , a significant increase of the bed capacity is obtained for all MB initial concentrations. When the flow rate increased further from  $100$  to  $150 \text{ mL min}^{-1}$ , the bed capacity was almost the same. This shows that increase of flow rate from  $50$  to  $100 \text{ mL min}^{-1}$  increases the surface diffusion phenomena in the bed column, which favors MB adsorption; further increase of the flow rate has no effect. In other

Table 2  
Fixed-bed adsorption parameters for the adsorption of MB onto acid-treated char at various conditions

Initial MB concentration $C_0$ (mg L <sup>-1</sup> )	Bed height (cm)	MB flow rate (mL min <sup>-1</sup> )	Breakthrough time, $t_b$ (min)	Bed exhausted time, $t_e$ (min)	$q_{total}$ (mg)	Bed capacity $q_{e,exp}$ (mg g <sup>-1</sup> )
10	15	50	760	940	444	1.48
10	15	100	560	680	618	2.06
10	15	150	370	456	651	2.17
20	15	50	580	850	741	2.47
20	15	100	420	670	1,137	3.79
20	15	150	280	440	1,104	3.68
40	15	50	410	480	897	2.99
40	15	100	260	345	1,155	3.85
40	15	150	150	230	1,122	3.74

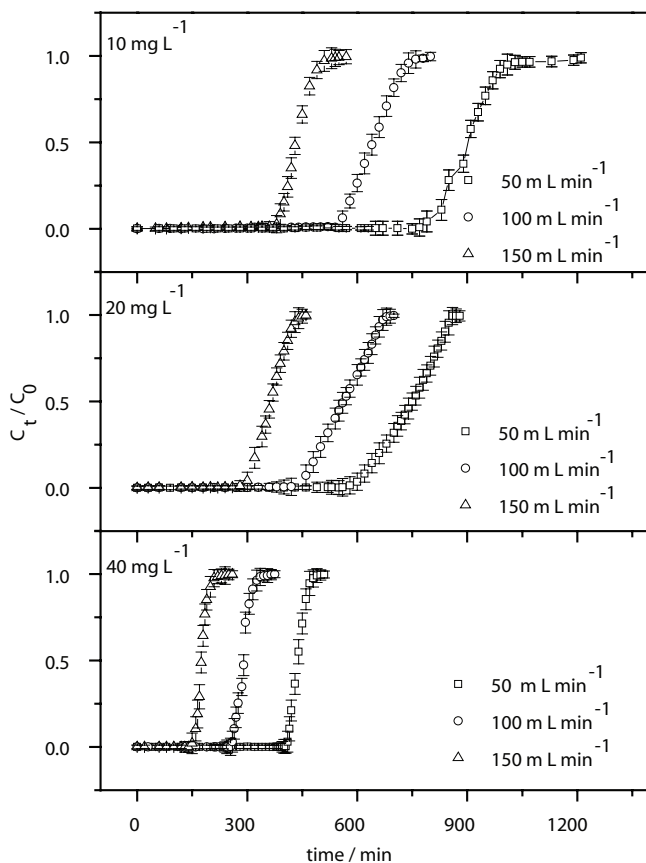


Fig. 7. Effects of various flow rates on the breakthrough curves at inlet MB concentrations of: (a) 10 mg L<sup>-1</sup>, (b) 20 mg L<sup>-1</sup> and (c) 40 mg L<sup>-1</sup>.

words, it seems that 100 mL min<sup>-1</sup> is the optimum flow rate for all MB initial concentrations to reach the appropriate balance between surface contact time and surface diffusion phenomena and to achieve the highest bed capacity [58]. Summarizing, all above results indicate that initial MB concentration and flow rate can affect the adsorption process and obviously the breakthrough curves. Similar behaviors have been observed by other researchers [1,3,55–61].

### 3.4. Adsorption models

The dynamic adsorption behavior of MB was examined using Yoon–Nelson, Thomas and Adams–Bohart models. The determined coefficients and the values of the models' parameters were obtained using non-linear curve simulation and linear regression analysis. The mathematical models were applied in order to investigate the mechanism of adsorption process and adsorbent affinity, as well as to model breakthrough behavior of MB onto CHTR.

#### 3.4.1. Yoon–Nelson model

The Yoon–Nelsons model parameters and correlation coefficients were determined from the slope and intercepts obtained from the linear regression analysis of  $\ln[C_t/(C_0 - C_t)]$  vs. time, as shown in Fig. 8, as well as from non-linear fitting of Eq. (5) to the experimental data and summarized in Table 3. As can be seen, the rate constant,  $k_{YN}$  increased with increasing inlet dye concentration and feed flow rate while the values of  $\tau$  decreased with both increasing flow rate and MB concentration. This happened because higher flow rate results in rapid saturation of CHTR in the column, and also because of limited adsorption. Moreover, the calculated  $\tau_{cal}$  values of the model were very similar with the time required for 50% adsorbent breakthrough from experiments ( $\tau_{exp}$ ).  $R^2$ , ARE and predicted model parameter values, as summarized in Table 3, indicated a good agreement between the experimental data and the predicted normalized concentration. In conclusion, Yoon–Nelson's model, which neglects the effect of axial dispersion, is suitable for representing the dynamic adsorption process and provided a good correlation between the effects of inlet MB concentration and flow rates.

#### 3.4.2. Thomas model

The Thomas model is one of the widely used models to simulate the adsorbent–solute interaction and to estimate the breakthrough curves. Fig. 9 shows the results of its linearized form (Eq. (8)) as the linear plot of  $\ln(C_0/C_t - 1)$  against time, at various operating conditions. The Thomas parameter rate constant,  $k_{th}$  and the equilibrium uptake,  $q_{th}$  were calculated with non-linear and linear fitting according to Eqs. (7) and (8), respectively, and are summarized in Table 4. As expected,

with the increase of initial MB concentration, the adsorption capacity  $q_{Th}$  increased while the Thomas constant  $k_{Th}$  decreased. The improved adsorption capacity was ascribed to the lower rate of mass transfer in column for higher concentration of MB, which had resulted in a longer contact time

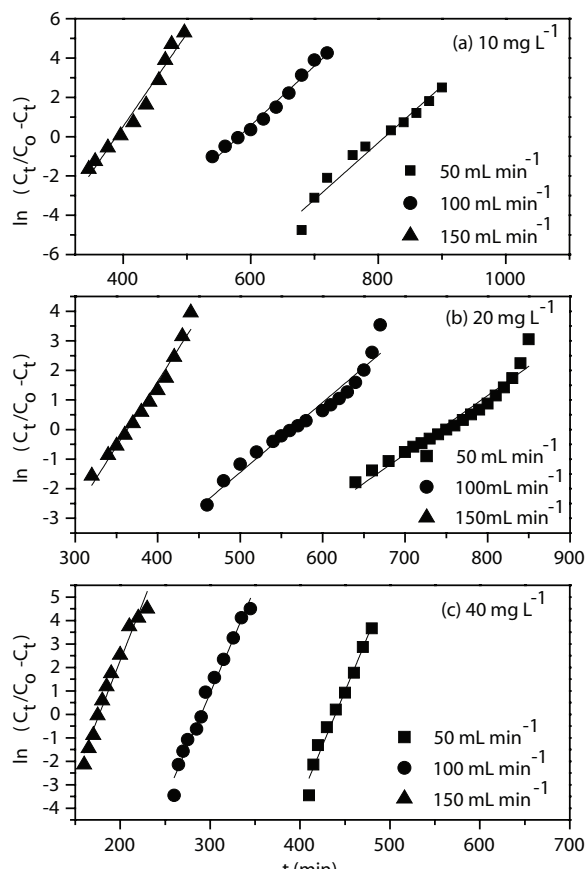


Fig. 8. Yoon–Nelson model linear plots for MB adsorption onto acid-treated pyrolytic char for dye inlet concentrations of: (a) 10 mg L<sup>-1</sup>, (b) 20 mg L<sup>-1</sup> and (c) 40 mg L<sup>-1</sup> at various flow rates (50, 100 and 150 mL min<sup>-1</sup>) and fixed bed height of 15 cm.

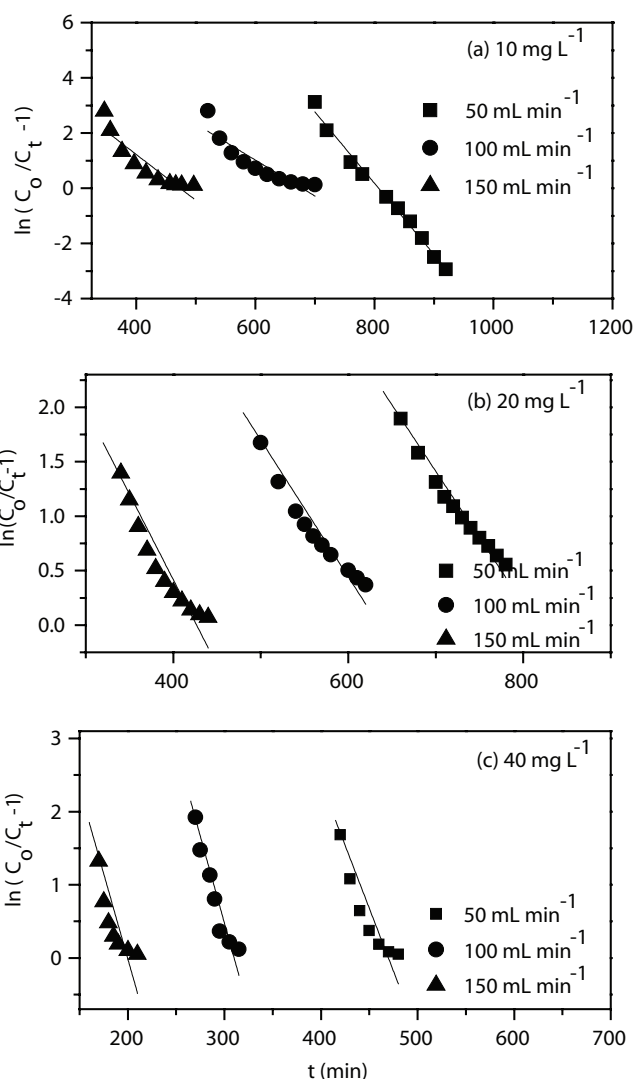


Fig. 9. Thomas model linear plots for MB adsorption onto acid-treated pyrolytic char for dye inlet concentrations of: (a) 10 mg L<sup>-1</sup>, (b) 20 mg L<sup>-1</sup> and (c) 40 mg L<sup>-1</sup> at various flow rates (50, 100 and 150 mL min<sup>-1</sup>) and fixed bed height of 15 cm.

Table 3

Yoon–Nelson parameters for the adsorption of MB on acid-treated char at different flow rates and inlet concentration using simulation and linear analysis

Q (mL min <sup>-1</sup> )	C <sub>0</sub> (mg L <sup>-1</sup> )	Z (cm)	M (g)	τ <sub>exp</sub> (min)	Non-linear			Linear			ARE (%)
					k <sub>YN</sub> (min <sup>-1</sup> )	τ <sub>cal</sub> (min)	R <sup>2</sup>	k <sub>YN</sub> (min <sup>-1</sup> )	τ <sub>cal</sub> (min)	R <sup>2</sup>	
50	10	15	300	902	0.026	901	0.9985	0.027	897	0.9690	11
100	10	15	300	640	0.027	642.9	0.9979	0.028	642	0.9796	9
150	10	15	300	433	0.047	435.5	0.9986	0.046	433	0.9819	6
50	20	15	300	745	0.026	745.6	0.9927	0.019	771.4	0.9444	12
100	20	15	300	563.2	0.029	563.7	0.9952	0.023	577.2	0.9521	10
150	20	15	300	360	0.050	364.3	0.9983	0.044	362.3	0.9716	10
50	40	15	300	437.8	0.088	438	0.9977	0.092	442.1	0.9756	10
100	40	15	300	288.6	0.096	288.9	0.9961	0.089	293.1	0.9808	7
150	40	15	300	175.5	0.131	175.9	0.9992	0.098	176.8	0.9647	9

Table 4

Thomas parameters for the adsorption of MB on acid-treated char at different flow rates and inlet concentration using simulation and linear analysis

Q (mL min <sup>-1</sup> )	C <sub>0</sub> (mg L <sup>-1</sup> )	Z (cm)	M (g)	q <sub>e,exp</sub> (mg g <sup>-1</sup> )	Non-linear			Linear			ARE (%)
					k <sub>Th</sub> × 10 <sup>-4</sup> (mL mg <sup>-1</sup> min <sup>-1</sup> )	q <sub>th,cal</sub> (mg g <sup>-1</sup> )	R <sup>2</sup>	k <sub>Th</sub> × 10 <sup>-4</sup> (mL mg <sup>-1</sup> min <sup>-1</sup> )	q <sub>th,linear</sub> (mg g <sup>-1</sup> )	R <sup>2</sup>	
50	0	15	300	1.48	29	1.48	0.9988	26	1.40	0.9690	15
100	0	15	300	2.06	31	2.07	0.9979	21	2.31	0.9105	18
150	10	15	300	2.17	48	2.18	0.9987	22	2.31	0.8837	10
50	20	15	300	2.47	9.8	2.48	0.9927	4.8	2.86	0.9523	11
100	20	15	300	3.79	11	3.81	0.9948	6.6	4.36	0.8508	8
150	20	15	300	3.68	22	3.71	0.9983	7.8	4.29	0.8885	16
50	40	15	300	2.99	31	2.99	0.9977	13	3.24	0.8266	15
100	40	15	300	3.85	29	3.82	0.9995	11	4.359	0.8813	26
150	40	15	300	3.74	35	3.73	0.9991	7.4	4.28	0.8337	24

between solute and adsorbent [1]. As the flow rate increased from 50 to 150 mL min<sup>-1</sup>, the values of q<sub>th</sub> decreased and k<sub>th</sub> increased. This is because the key driving force for adsorption is the concentration difference between the MB on the CHTR and MB in the solution. It is also observed that the calculated from the non-linear fitting q<sub>th</sub> values are in close agreement with the corresponding data obtained experimentally in comparison with the q<sub>th</sub> values calculated via linear fitting. On the other hand, the correlation coefficient values R<sup>2</sup> of linear fitting, which are in the range of 0.83–0.97, and the low ARE values provided also a good fitting of the model to the experimental data. Moreover, based on the surface characteristics of CHTR reported previously, the adsorption mechanisms of MB can be attributed to cation–π interactions between the cationic dye and the electron-rich graphitic sheets and electrostatic attraction of opposite charges between anionic carboxyl groups and cationic dye ions in solution. Taking also into account the pseudo-second-order adsorption kinetics, the assumptions of Thomas model can be satisfied, and the model is suitable to describe MB adsorption in the fixed bed of CHTR. Linear and non-linear regression are both suitable to predict the breakthrough curves using Thomas model parameters; however, the non-linear method is better. Similar conclusion has been reported elsewhere [62] for MB adsorption into natural zeolite.

#### 3.4.3. Adams–Bohart model

Adams–Bohart model was also applied to describe the experimental data of the breakthrough curves. The parameters, adsorption capacity (N<sub>0</sub>) and kinetic constant (k<sub>AB</sub>), from the Adams–Bohart model were obtained from the plot ln(C<sub>t</sub>/C<sub>0</sub>) against time, at various operating conditions as shown in Fig. 10 and listed in Table 5. As can be seen in Table 5, the values of rate constant k<sub>AB</sub> increased with the increase of flow rate and decreased with the increase of the initial MB concentration, indicating that the dynamic adsorption system was governed by external mass transfer resistance in the initial stage of the adsorption process [58,63]. The maximum value of adsorption capacity N<sub>0</sub> was calculated as 2,889 mg L<sup>-1</sup> for the highest inlet concentration of 40 mg L<sup>-1</sup> and for a feed flow rate

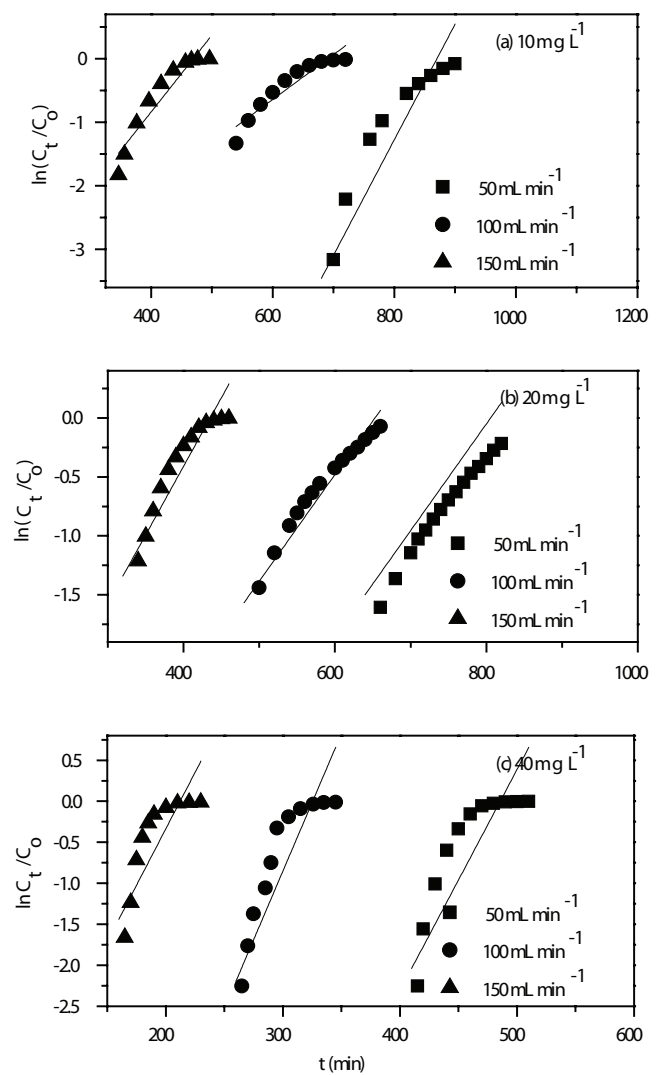


Fig. 10. Adams–Bohart model linear plots for MB adsorption onto acid-treated pyrolytic char for dye inlet concentrations of: (a) 10 mg L<sup>-1</sup>, (b) 20 mg L<sup>-1</sup> and (c) 40 mg L<sup>-1</sup> at various flow rates (50, 100 and 150 mL min<sup>-1</sup>) and fixed bed height of 15 cm.

Table 5

Adams–Bohart parameters for the adsorption of MB on acid-treated char at different flow rates and inlet concentration using simulation and linear analysis

Q (mL min <sup>-1</sup> )	C <sub>0</sub> (mg L <sup>-1</sup> )	Z (cm)	M (g)	k <sub>AB</sub> × 10 <sup>-4</sup> (L mg <sup>-1</sup> min <sup>-1</sup> )	N <sub>0</sub> (mg L <sup>-1</sup> )	R <sup>2</sup>	k <sub>AB</sub> × 10 <sup>-4</sup> (L mg <sup>-1</sup> min <sup>-1</sup> )	N <sub>0</sub> (mg L <sup>-1</sup> )	R <sup>2</sup>	ARE (%)
50	10	15	300	29	1,035	0.9985	15	1,035	0.7745	35
100	10	15	300	27.5	1,619	0.9979	17	1,688	0.9371	53
150	10	15	300	47.5	1,623	0.9986	15	1,791	0.9416	28
50	20	15	300	9.65	1,870	0.9933	4.2	2,103	0.9715	61
100	20	15	300	11	2,847	0.9952	5.2	3,246	0.8858	47
150	20	15	300	20	2,729	0.9983	6.9	3,180	0.9092	38
50	40	15	300	22	2,184	0.9987	11	2,331	0.7470	34
100	40	15	300	24.2	2,889	0.9995	8.4	3,256	0.7135	83
150	40	15	300	33	2,634	0.9991	6.8	3,182	0.6408	91

of 100 mL min<sup>-1</sup>. The correlation coefficients R<sup>2</sup> of non-linear fitting are in the range of 0.9933–0.9991 a fact that reveals the higher accuracy of N<sub>0</sub> and K<sub>AB</sub> values compared with the same values calculated from linear fitting. R<sup>2</sup> and ARE values are given in Table 5. As for the R<sup>2</sup> for linear fitting, the values show distribution between 0.64 and 0.97. Nevertheless, most of the R<sup>2</sup> are less than 0.9, which indicates that the data does not fit sufficiently well into the model. In addition, ARE analysis values (Table 5) are the highest ones from all other models. Thus, R<sup>2</sup> and ARE analysis values of Adams–Bohart model suggest a lack-of-fit to the experimental data. This happens because the Adams–Bohart model is used to describe the initial part of the breakthrough curve [58]. As a result, it can be confirmed that the Adams–Bohart model is unsuitable to explain the overall adsorption behavior of the column.

### 3.5. Desorption studies

Desorption studies were conducted to elucidate the nature of adsorption as well as the recycling of the spent adsorbent. The adsorbed MB dye cannot be desorbed using deionized neutral pH water; thus, the sorption of the dye on the adsorbent cannot be ascribed to weak bonds. On the contrary, acid solution can desorb the dye as shown in desorption–elution curves depicted in Fig. 11. A sharp increase of MB concentration in the column effluent is observed at the first 30 min followed by a continuous decrease thereafter. The total desorption time of MB approximates 800 min, which is close to the experimental time adsorption cycle. Desorption of MB by acid solution indicates that MB adsorption onto the CHTR proceeds probably through physisorption mechanisms as suggested previously. The breakthrough curves after three consecutive adsorption cycles are shown in Fig. 12. It can be observed that the breakthrough curves shifted to the left, toward the C<sub>t</sub>/C<sub>0</sub> axis, indicating that a lower amount of dye was removed for the second and third adsorption cycle. On other words, breakthrough time and the efficiency of adsorption column decreased as the adsorption cycles increased. About 72% and 64% of the initial column adsorption capacity was maintained for the second and third adsorption cycle, respectively, while about 90% of the adsorption capacity was maintained between the second and third adsorption cycle.

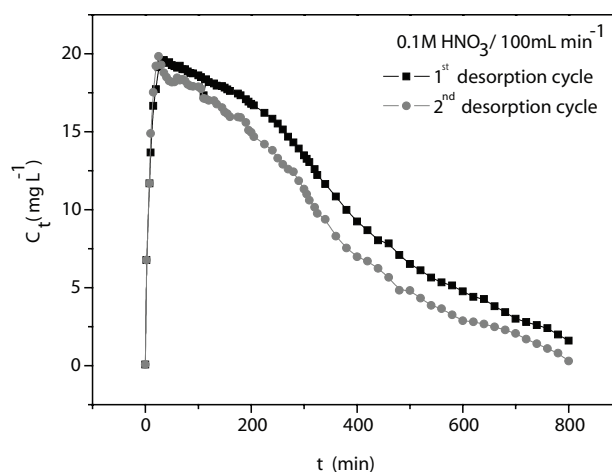


Fig. 11. Elution curve for desorption of MB dye by 0.1 M HNO<sub>3</sub> (initial dye concentration for adsorption cycle: 20 mg L<sup>-1</sup>; adsorbent bed length: 15 cm; flow rate: 10 mL min<sup>-1</sup>).

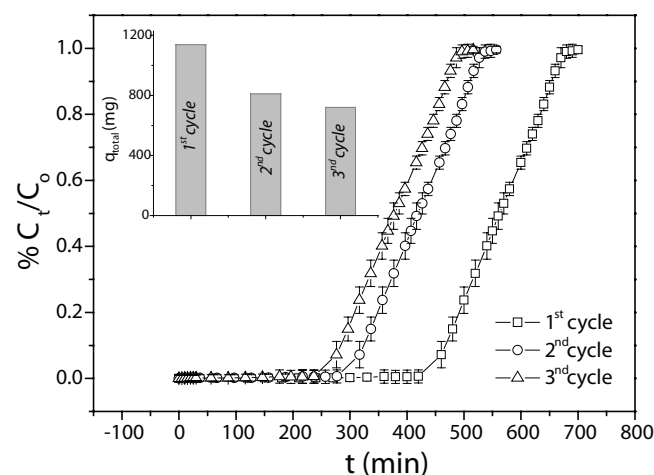


Fig. 12. Breakthrough curves of MB onto CHTR and regenerated CHTR by 0.1 M HNO<sub>3</sub> (initial dye concentration: 20 mg L<sup>-1</sup>; adsorbent bed length: 15 cm; flow rate: 10 mL min<sup>-1</sup>).

### 3.6. Comparison with other adsorbents

Tan et al. [3] and Foo and Hameed [55] studied the adsorption of MB onto palm oil shell-based activated carbon at continuous fixed-bed columns with 6 cm bed height and 20 mL min<sup>-1</sup> flow rate, and they determined the highest bed capacity as 133.13 and 40.86 mg g<sup>-1</sup> using initial dye concentration of 150 and 100 mg L<sup>-1</sup>, respectively. Similar trends were obtained for the adsorption of MB onto activated carbon derived from peach stone shells by chemical activation with a column adsorption capacity of 71.80 mg g<sup>-1</sup> [64]. Li et al. [59] found a maximum column MB adsorption capacity of 103.58 mg g<sup>-1</sup> for paper mill sewage sludge-based activated carbon. Moreover, adsorption capacities of 12.06 mg g<sup>-1</sup> [59] and 240 mg g<sup>-1</sup> [65] were obtained with coal-based commercial activated carbon and commercial activated carbon Filtrasorb F300, respectively. Finally, some activated carbons prepared from other sources such as textile wastes (polyamide, polyester and cotton) [66], as well as natural sorbent materials such as zeolites [62], showed lower adsorption capacities being 7 and 4.36 mg g<sup>-1</sup>, respectively.

A comparison of the bed capacity of CHTR (3.85 mg g<sup>-1</sup>) for MB removal with the above values of the literature showed that activated carbons exhibited higher to comparable adsorption capacities while other natural sorbent materials showed similar adsorption capacities. Taking into account that tire char production process is simple compared with commercial or other activated carbons, the ample availability of waste tire feedstock and the alternative waste tire management solution provided by tire pyrolysis, CHTR can be considered as a promising adsorbent for the removal of MB dye in fixed-bed column.

## 4. Conclusions

This study shows that adsorption of MB in aqueous solutions can be achieved with acid-treated PTC as an adsorbent in a fixed-bed column. The surface properties of CHTR revealed mostly microcrystalline graphitic structure with macroporous/nonporous characteristics and acidic groups on its surface due to the treatment with nitric acid. The adsorption in the continuous adsorption system depends on the initial MB concentration and feed flow rate at a constant bed height. As the flow rate and MB inlet concentration increased, the breakthrough curve became steeper, while the adsorption capacity increased. Three kinetic models, Thomas, Yoon–Nelson and Adams–Bohart, were applied to fit the experimental data. The Thomas and Yoon–Nelson model predictions were in very good agreement with the experimental results for all the process parameters studied, as indicated by the high values of correlation coefficient  $R^2$  and the low ARE values, thus suggesting that they were suitable to describe the dynamic adsorption behavior of MB onto CHTR.  $R^2$  and ARE values for Adams–Bohart model did not provide a good fit to the experimental data. For the fixed 15 cm of adsorbent-bed height employed in this study, the adsorbent exhibited the maximum bed capacity of 3.85 mg g<sup>-1</sup> at a flow rate of 100 mL min<sup>-1</sup> and initial MB concentration of 40 mg L<sup>-1</sup>. The desorption of MB and the regeneration of the column can be performed by acid aqueous solutions; however, the efficiency of adsorption column decreased as

the adsorption cycles increased reaching about 64% of the initial adsorption capacity for the third adsorption cycle.

## Acknowledgment

This work is financially supported by the “SYNERGASIA” Program 11SYN\_5\_682 (O.P. Competitiveness & Entrepreneurship; EPAN II), ROP Macedonia, Thrace, ROP Crete and Aegean Islands, ROP Thessaly, Mainland Greece, Epirus, ROP Attica.

## References

- [1] W. Zhang, L. Dong, H. Yan, H. Li, Z. Jiang, X. Kan, H. Yang, A. Li, R. Cheng, Removal of methylene blue from aqueous solutions by straw based adsorbent in a fixed-bed column, *Chem. Eng. J.*, 173 (2011) 429–436.
- [2] N. Mathur, P. Bhatnager, P. Bakre, Assessing mutagenicity of textile dyes from Pali (Rajasthan) using Ames bioassay, *Appl. Ecol. Environ. Res.*, 4 (2006) 111–118.
- [3] I.A.W. Tan, A.L. Ahmad, B.H. Hameed, Adsorption of basic dye using activated carbon prepared from oil palm shell: batch and fixed bed studies, *Desalination*, 225 (2008) 13–28.
- [4] V. Vadivelan, K.V. Kumar, Equilibrium, kinetics, mechanism and process design for the sorption of methylene blue onto rice husk, *J. Colloid Interface Sci.*, 286 (2005) 90–100.
- [5] E.L.K. Mui, W.H. Cheung, G. McKay, Tire char preparation from waste tyre rubber for dye removal from effluents, *J. Hazard. Mater.*, 175 (2010) 151–158.
- [6] M.A. Al-Ghouti, M.A.M. Khraisheh, M.N.M. Ahmad, S.J. Allen, Adsorption behavior of methylene blue onto Jordanian diatomite: a kinetic study, *J. Hazard. Mater.*, 165 (2009) 589–598.
- [7] T. Robinson, R. Marchant, P. Nigam, Remediation of dyes in textile effluent: a critical review on current treatment technologies with a proposed alternative, *Bioresour. Technol.*, 77 (2001) 247–255.
- [8] M.T. Uddin, M. Rukanuzzaman, M.M.M. Khan, M.A. Islam, Adsorption of methylene blue from aqueous solution by jackfruit (*Artocarpus heterophyllus*) leaf powder: a fixed-bed column study, *J. Environ. Manage.*, 90 (2009) 3443–3450.
- [9] R. Han, D. Ding, Y. Xu, W. Zou, Y. Wang, Y. Li, L. Zou, Use of rice husk for the adsorption of congo red from aqueous solution in column mode, *Bioresour. Technol.*, 99 (2008) 2938–2946.
- [10] S.S. Baral, N. Das, T.S. Ramulu, S.K. Sahoo, S.N. Das, G.R. Chaudhury, Removal of Cr(VI) by thermally activated weed *Salvinia cucullata* in a fixed-bed column, *J. Hazard. Mater.*, 161 (2009) 1427–1435.
- [11] E.I. Unuabonah, B.I. Olu-Owolabi, E.I. Fasuyi, K.O. Adebowale, Modeling of fixed-bed column studies for the adsorption of cadmium onto novel polymer–clay composite adsorbent, *J. Hazard. Mater.*, 179 (2010) 415–423.
- [12] Z. Wang, Y. Tian, X. Wang, Adsorption performance to methylene blue by non-activated tire-based pyrolytic char, *Appl. Mech. Mater.*, 508 (2014) 35–39.
- [13] F. Rozada, M. Otero, J.B. Parra, A. Moran, A.I. Garcia, Producing adsorbents from sewage sludge and discarded tyres: characterization and utilization for the removal of pollutants from water, *Chem. Eng. J.*, 114 (2005) 161–169.
- [14] E.L.K. Mui, W.H. Cheung, M. Valix, G. McKay, Dye adsorption onto activated carbons from tyre rubber waste using surface coverage analysis, *J. Colloid Interface. Sci.*, 347 (2010) 290–300.
- [15] E.M. Vizuete, A.M. Garcia, A.N. Gisbert, C.F. Gonzalez, V.G. Serrano, Adsorption of mercury by carbonaceous adsorbents prepared from rubber of tyre wastes, *J. Hazard. Mater.*, 119 (2005) 231–238.
- [16] G. McKay, M.J. Bino, A.R. Altamemi, The adsorption of various pollutants from aqueous solutions onto activated carbon, *Water Res.*, 19 (1985) 491–495.
- [17] N. Antoniou, A. Zabaniotou, Experimental proof of concept for a sustainable end of life tires pyrolysis with energy and porous materials production, *J. Clean. Prod.*, 101 (2015) 323–336.

- [18] H. Teng, M.A. Serio, M.A. Whittowicz, R. Bassilakis, P.R. Solomon, Reprocessing of used tires into activated carbon and other products, *Ind. Eng. Chem. Res.*, 34 (1995) 3102–3111.
- [19] P. Ariyadejwanich, W. Tanthapanichakoon, K. Nakagawa, S.R. Mukai, H. Tamon, Preparation and characterization of mesoporous activated carbon from waste tires, *Carbon*, 41 (2003) 157–164.
- [20] V.K. Gupta, I. Ali, V.K. Saini Suh, Removal of Rhodamine B, fast green, and methylene blue from wastewater using red mud, an aluminum industry waste, *Ind. Eng. Chem. Res.*, 43 (2004) 1740–1747.
- [21] Z. Eren, F.N. Acar, Adsorption of Reactive Black 5 from an aqueous solution: equilibrium and kinetic studies, *Desalination*, 194 (2006) 1–10.
- [22] V.K. Gupta, A. Mittal, L. Krishnan, J. Mittal, Adsorption treatment and recovery of the hazardous dye, Brilliant Blue FCF, over bottom ash and de-oiled soya, *J. Colloid Interface Sci.*, 293 (2006) 16–26.
- [23] B. Armagan, T. Mustafa, M.S. Celik, Equilibrium studies on the adsorption of reactive azo dyes into zeolite, *Desalination*, 170 (2004) 33–39.
- [24] R.P. Han, Y.F. Wang, P. Han, J. Shi, J. Yang, Y.S. Lu, Removal of methylene blue from aqueous solution by chaff in batch mode, *J. Hazard. Mater.*, 137 (2006) 550–557.
- [25] K.V. Kumar, S. Sivanesan, Equilibrium data, isotherm parameters and process design for partial and complete isotherm of methylene blue onto activated carbon. *J. Hazard. Mater.*, 131 (2006) 237–244.
- [26] B. Acevedo, C. Barriocanal, Texture and surface chemistry of activated carbons obtained from tyre wastes, *Fuel Process. Technol.*, 134 (2015) 275–283.
- [27] V. Makrigianni, A. Giannakas, Y. Deligiannakis, I. Konstantinou, Adsorption of phenol and methylene blue from aqueous solutions by pyrolytic tire char: equilibrium and kinetic studies, *J. Environ. Chem. Eng.*, 3 (2015) 574–582.
- [28] V. Makrigianni, A. Giannakas, C. Daikopoulos, Y. Deligiannakis, I. Konstantinou, Preparation, characterization and photocatalytic performance of pyrolytic-tire-char/TiO<sub>2</sub> composites, toward phenol oxidation in aqueous solutions, *Appl. Catal., B*, 174 (2015) 244–252.
- [29] R. Acosta, V. Fierro, A. Martinez de Yuso, D. Nabarlatz, A. Celzard, Tetracycline adsorption onto activated carbons produced by KOH activation of tyre pyrolysis char, *Chemosphere*, 149 (2016) 168–176.
- [30] C. Troca-Torrado, M. Alexandre-Franco, C. Fernández-González, M. Alfaro-Domínguez, V. Gómez-Serrano, Development of adsorbents from used tire rubber: their use in the adsorption of organic and inorganic solutes in aqueous solution, *Fuel Process. Technol.*, 92 (2011) 206–212.
- [31] T.A. Saleh, V.K. Gupta, Processing methods, characteristics and adsorption behaviour of tire derived carbons: a review, *Adv. Colloid Interface Sci.*, 211 (2014) 93–101.
- [32] A. Shahtalebi, M.M. Sarrafraideh, G. McKay, An adsorption diffusion model for removal of copper(II) from aqueous solution by pyrolytic tyre char, *Desal. Wat. Treat.*, 51 (2013) 5664–5673.
- [33] H.P. Boehm, Some aspects of the surface chemistry of carbon blacks and other carbons, *Carbon*, 32 (1994) 759–769.
- [34] K. Bourikas, J. Vakros, C. Kordulis, A. Lycourghiotis, Potentiometric mass titrations: experimental and theoretical establishment of a new technique for determining the point of zero charge (PZC) of metal (hydr)oxides, *J. Phys. Chem. B*, 107 (2003) 9441–9451.
- [35] G.S. Bohart, E.Q. Adams, Behavior of charcoal towards chlorine, *J. Chem. Soc.*, 42 (1920) 523–544.
- [36] Y.H. Yoon, J.H. Nelson, Application of gas adsorption kinetics. Part 1. A theoretical model for respirator cartridge service time, *Am. Ind. Hyg. Assoc. J.*, 45 (1984) 509–516.
- [37] H.C. Thomas, Heterogeneous ion exchange in a flowing system, *J. Am. Chem. Soc.*, 66 (1944) 1664–1666.
- [38] E.M. Suuberg, I. Aarna, The Nature of Porosity in Carbons Derived from Scrap Automobile Tires, Division of Engineering, Brown University Providence, RI 02912, USA.
- [39] A.M. Fernandez, C. Barriocanal, R. Alvarez, Pyrolysis of a waste from the grinding of scrap tyres, *J. Hazard. Mater.*, 203–204 (2012) 236–243.
- [40] R. Helleur, N. Popovic, M. Ikura, M. Stanculescu, D. Liu, Characterisation and potential applications of pyrolytic char from ablative pyrolysis of used tires, *J. Anal. Appl. Pyrolysis*, 58–59 (2001) 813–824.
- [41] A. Zabaniotou, G. Stavropoulos, Pyrolysis of used automobile tires and residual char utilization, *J. Anal. Appl. Pyrolysis*, 70 (2003) 711–722.
- [42] G.S. Miguel, G.D. Fowler, M. Dall’Orso, C.J. Sollars, Porosity and surface characteristics of activated carbons produced from waste tyre rubber, *J. Chem. Technol. Biotechnol.*, 77 (2001) 1–8.
- [43] P. Hadi, K.Y. Yeung, J. Guo, H. Wang, G. McKay, Sustainable development of tyre char-based activated carbons with different textural properties for value-added applications, *J. Environ. Manage.*, 170 (2016) 1–7.
- [44] P.T. Williams, Pyrolysis of waste tyres: a review, *Waste Manage.*, 33 (2013) 1714–1728.
- [45] S.Q. Li, Q. Yao, Y. Chi, J.H. Yan, K.F. Cen, Pilot-scale pyrolysis of scrap tires in a continuous rotary kiln reactor, *Ind. Eng. Chem. Res.*, 43 (2004) 5133–5145.
- [46] F.A. López, T.A. Centeno, O. Rodríguez, F.J. Alguacil, Preparation and characterization of activated carbon from the char produced in the thermolysis of granulated scrap tyres, *J. Air Waste Manage. Assoc.*, 63 (2013) 534–544.
- [47] F. Lian, F. Huang, W. Chen, B. Xing, L. Zhu, Sorption of a polar and polar organic contaminants by waste tire rubber and its chars in single- and bi-solute systems, *Environ. Pollut.*, 159 (2011) 850–857.
- [48] Y. Li, Q. Du, T. Liu, X. Peng, J. Wang, J. Sun, Y. Wang, S. Wu, Z. Wang, Y. Xia, L. Xia, Comparative study of methylene blue dye adsorption onto activated carbon, graphene oxide, and carbon nanotubes, *Chem. Eng. Res. Des.*, 91 (2013) 361–368.
- [49] W.J. Weber, J.X. Tang, Q.G. Huang, Development of engineered natural organic sorbents for environmental applications. 1. Materials, approaches, and characterizations, *Environ. Sci. Technol.*, 40 (2006) 1650–1656.
- [50] H. Deng, L. Yang, G.H. Tao, J.L. Dai, Preparation and characterization of activated carbon from cotton stalk by microwave assisted chemical activation application in methylene blue adsorption from aqueous solution, *J. Hazard. Mater.*, 166 (2009) 1514–1521.
- [51] R. Ji, K. Yu, L.-L. Lou, C. Zhang, Y. Han, S. Pan, S. Liu, Chiral Mn(III) salen complexes immobilized directly on pyrolytic waste tire char for asymmetric epoxidation of unfunctionalized olefins, *Inorg. Chem. Commun.*, 25 (2012) 65–69.
- [52] N. Ben Douissa, L. Bergaoui, S. Mansouri, R. Khiari, M.F. Mhenni, Macroscopic and microscopic studies of methylene blue sorption onto extracted celluloses from *Posidonia oceanica*, *Ind. Crops Prod.*, 45 (2013) 106–113.
- [53] J. Goel, K. Kadirvelu, C. Rajagopal, V.K. Garg, Removal of lead(II) by adsorption using treated granular activated carbon: batch and column studies, *J. Hazard. Mater.*, 125 (2005) 211–220.
- [54] E. Malko, Y. Nuhoghi, Removal of Ni(II) ions from aqueous solutions using waste of tea factory: adsorption on a fixed-bed column, *J. Hazard. Mater.*, 135 (2006) 328–336.
- [55] K.Y. Foo, B.H. Hameed, Dynamic adsorption behavior of methylene blue onto oil palm shell granular activated carbon prepared by microwave heating, *Chem. Eng. J.*, 203 (2012) 81–87.
- [56] R. Han, Y. Wang, W. Yu, W. Zou, J. Shi, H. Liu, Biosorption of methylene blue from aqueous solution by rice husk in a fixed bed column, *J. Hazard. Mater.*, 141 (2007) 713–718.
- [57] D.C.K. Ko, J.F. Porter, G. McKay, Optimised correlations for the fixed bed adsorption of metal ions on bone char, *Chem. Eng. Sci.*, 55 (2000) 5819–5829.
- [58] O. Ozdemir, M. Turan, A.Z. Turan, A. Faki, A.B. Engin, Feasibility analysis of color removal from textile dyeing wastewater in a fixed-bed column system by surfactant-modified zeolite (SMZ), *J. Hazard. Mater.*, 166 (2009) 647–654.
- [59] W. Li, Y. Qinyan, T. Peng, M. Zuo hao, B. Gao, J. Li, X. Xu, Adsorption characteristics of dyes in columns of activated carbon prepared from paper mill sewage sludge, *Chem. Eng. J.*, 178 (2011) 197–203.

- [60] A.B. Albadarin, C. Mangwandi, A.H. Al-Muhtaseb, G.M. Walker, S.J. Allen, M.N.M. Ahmad, Modelling and fixed bed column adsorption of Cr(VI) onto orthophosphoric acid-activated lignin, *Chin. J. Chem. Eng.*, 20 (2012) 469–477.
- [61] S. Sugashini, K. Mohamed, M.S. Begum, Performance of ozone treated rice husk carbon (OTRHC) for continuous adsorption of Cr (VI) ions from synthetic effluent, *J. Environ. Chem. Eng.*, 1 (2013) 79–85.
- [62] R. Han, Y. Wang, W. Zou, Y. Wang, J. Shi, Comparison of linear and nonlinear analysis in estimating the Thomas model parameters for methylene blue adsorption onto natural zeolite in fixed-bed column, *J. Hazard. Mater.*, 145 (2007) 331–335.
- [63] Z. Aksu, F. Gonen, Biosorption of phenol by immobilized activated sludge in a continuous packed bed: prediction of breakthrough curves, *Process Biochem.*, 39 (2004) 599–613.
- [64] A.A. Attia, B.S. Girgis, N.A. Fathy, Removal of methylene blue by carbons derived from peach stones by  $H_3PO_4$  activation: batch and column studies, *Dyes Pigm.*, 76 (2008) 282–289.
- [65] G.G. Stavropoulos, A.A. Zabaniotou, Production and characterization of activated carbons from olive-seed waste residue, *Microporous Mesoporous Mater.*, 82 (2005) 79–85.
- [66] Ç. Sarici-Özdemir, Removal of methylene blue by activated carbon prepared from waste in a fixed-bed column, *Particul. Sci. Technol.*, 32 (2014) 311–318.